論文 / 著書情報
Article / Book Information

Title	Two-parameter analysis of fatigue crack growth behavior in structural acrylic adhesive joints
Authors	Yu Sekiguchi, Keiji Houjou, Kazumasa Shimamoto, Chiaki Sato
Citation	Fatigue & Fracture of Engineering Materials & Structures, Vol. 46, Issue 3, pp. 909-923
Pub. date	2022, 11
DOI	https://doi.org/10.1111/ffe.13908
Creative Commons	Information is in the article.

Received: 22 June 2022 | Revised: 5 November 2022 | Accepted: 15 November 2022

DOI: 10.1111/ffe.13908

ORIGINAL ARTICLE

FFEMS Fatigue & Fracture of Engineering Materials & Structures WILEY

Two-parameter analysis of fatigue crack growth behavior in structural acrylic adhesive joints

Yu Sekiguchi[1] | Keiji Houjou[2] | Kazumasa Shimamoto[2] | Chiaki Sato[1]

[1]Institute of Innovative Research, Tokyo Institute of Technology, Yokohama, Japan

[2]Nanomaterials Research Institute, The National Institute of Advanced Industrial Science and Technology, Tsukuba, Japan

Correspondence
Yu Sekiguchi, Institute of Innovative Research, Tokyo Institute of Technology, 4259 Nagatsuta-cho, Midori-ku, Yokohama, 226-8503 Japan.
Email: sekiguchi.y.aa@m.titech.ac.jp

Funding information
New Energy and Industrial Technology Development Organization

Abstract

Conducting displacement-controlled fatigue double cantilever beam tests of a structural acrylic adhesive, two different slopes were observed in the fatigue crack growth (FCG) relationship of the FCG rate versus the strain energy release rate (SERR) parameters depending on the loading conditions. Because fatigue is a two-parameter problem where stress waveforms contain cyclic and monotonic terms, the contribution of each term toward FCG needs to be clarified. Therefore, each slope was explained using SERR with load range and mean load. In addition, cases were observed where the slope changed with an increasing number of cycles. Accordingly, the FCG rate changes. Understanding the phenomenon is important to estimate the crack position from an engineering point of view. Therefore, FCG was categorized into three types using amplitude and mean displacement. After a sufficient number of fatigue cycles, amplitude played a more dominant role than *R*-ratio or mean displacement to determine crack location.

KEYWORDS

bonded joints, crack driving force, creep, fatigue fracture toughness, structural adhesive

1 | INTRODUCTION

Nowadays, joining technology is essential to the manufacturing industry, and adhesive bonding is one of the most promising methods in joining technology; consequently, most products use adhesives. Hence, the reliability of adhesive joints is becoming increasingly important. Because most adhesives are composed of polymers, their bonding performance is greatly affected by the conditions of use. Therefore, performance evaluation of adhesives in harsh environments is crucial and requires implementing several types of test methods under various conditions.

Strength and toughness are the two major mechanical evaluation criteria of adhesive joints. Under fatigue loads, the curve of strength versus number of cycles (S–N curve) and fatigue crack growth (FCG) relationship (crack propagation per cycle versus fracture mechanics parameter) are used for strength and toughness evaluations, respectively. However, considering fatigue tests of adhesive joints, standards have been set only for strength evaluation[1,2] and not for toughness evaluation. Test methods for fiber-reinforced plastics (FRPs) are often applied to adhesive joint evaluations because the evaluation of FRPs has several similarities with that of adhesively bonded joints. For FRPs, one standard exists for toughness

evaluation.[3] However, this standard aims at determining mode I delamination growth onset; it does not discuss the FCG relationship. Therefore, there is a push to develop standard test procedures for deriving the FCG relationship of composites through round-robin activities by the American Society for Testing and Materials International Committee D30[4] and the European Structural Integrity Society Technical Committee 4.[5–8] Regarding the mode I fatigue toughness tests of adhesives, various discussions on the test procedure and the interpretation of the results are being undertaken, and further progress is expected through more research. To this end, this study focuses on two aspects of mode I fatigue toughness tests for adhesives: adhesive type and loading condition.

Among resins, epoxy resins have reigned as the major base polymer of structural adhesives for decades. Indeed, most studies investigating FCG relationship in adhesive joints deal with epoxy adhesives.[9–25] In addition to reporting the FCG behavior of the adhesive itself, the effects of bonding thickness,[9,23] humidity or wetness,[11–13,18,21] loading,[14,19,20,24] and substrate[15,17,25] have been investigated. However, in recent years, other types of polymers, such as acrylic or polyurethane, have been gaining prevalence as base polymers for structural adhesives. The fracture toughness response to dynamicity is highly dependent on the type of adhesive.[26] Because the same holds true for fatigue behavior,[27] investigating the FCG behavior of non-epoxy adhesives is critical.

Second-generation acrylic (SGA) adhesives are two-component adhesives that cure rapidly at room temperature, possess excellent strength and toughness, and are one of the typical structural acrylic adhesives.[28] Rubber is micro-dispersed in the acrylic resin due to phase separation in a so-called "sea-island structure" to achieve high ductility and toughness.[29–32] Moreover, acrylic adhesives are less susceptible to surface conditions than epoxy adhesives and have a good adhesion to slightly oily or unprepared surfaces.[33] Structural acrylic adhesives are often used for manufacturing large-sized structures in the marine, wind, and transportation industries due to their ease of usability and handling. Because large structures are always subject to periodic loads, fatigue performance of structural acrylic adhesives is important. Therefore, the effects of substrate thickness,[34] substrate materials,[35] adhesive thickness,[36] mode mixity,[37] and R-ratio[36,38] on the FCG behavior have been discussed for structural acrylic adhesives. However, research on this topic is scarce compared to epoxy adhesives, and further understanding will significantly help in predicting the fatigue life of joints more accurately.

The effect of cyclic loading parameters on FCG is another critical aspect of fatigue discussion. How much the crack propagates changes when loading conditions, such as the amplitude or mean value of the stress wave, vary. To explain it, fatigue is sometimes dealt with as a two-parameter problem.[39–42] It is well established that increasing the mean load adversely affects the fatigue strength of adhesive joints.[43] However, the FCG behavior with respect to loading conditions is complex because several factors possibly influence the mean load.[44] For instance, creep promotes crack growth in polymers. Therefore, creep effect has been suggested as a possible reason for the deviation of the FCG relationship at higher loads for an epoxy adhesive, but a clear explanation has not been proposed.[20] Furthermore, a large deviation due to loading level has been reported for the SGA adhesive.[36] Therefore, it is necessary to consider not only the effect of the R-ratio but also the effect of other waveform parameters on the FCG behavior.

In this study, displacement-controlled fatigue double cantilever beam (DCB) tests were performed by varying multiple waveform parameters to deepen the understanding of the trends in the FCG relationship of a structural acrylic adhesive.

2 | APPLICATION OF FRACTURE MECHANICS TO FCG

2.1 | Derivation of strain energy release and FCG rates

Using the simple beam theory, the strain energy release rate (SERR, G) of DCB tests is given as

$$G = \frac{P^2 a^2}{bEI}, \tag{1}$$

where P is the applied load, a is the crack length, b and E are the width and Young's modulus of the substrate, respectively, and I is the moment of inertia of the substrate cross-section. It should be noted that accurate measurement of the crack length is challenging in DCB tests. Recently, crack measurement systems using digital image correlation technique[45] and mechanoluminescence[46] have been developed, but in general, difficulties still remain. In addition, when optically measured crack length is used for the calculation of SERR, crack length correction is required because of the effects such as root rotation[47] and fracture process zone[48] at the crack front. To this end, a data reduction approach using beam theory, the so-called compliance-based beam method (CBBM), has been proposed.[48] Using this CBBM method, SERR can be verifiably derived for various types of adhesives from brittle to soft without the crack length measurement.[49] Moreover, it was theoretically verified that

the equivalent crack length calculated using the CBBM almost agrees with the sum of crack length and crack length correction, $a+|\Delta|$, if the adhesive exhibits elastoplastic behavior.[50] In the case of the SGA used in this study, it behaves almost elastoplastic and it was experimentally confirmed that the crack length correction and the gap between the optically measured crack and equivalent crack length had similar value under static and dynamic loading conditions.[51] Fernández et al also confirmed in the fatigue tests that the optically measured crack length and equivalent crack length show a similar tendency as a function of a number of cycles, in addition to the existence of a constant gap associated with the crack length correction.[16] Consequently, no further crack length adjustments are required when using CBBM. After neglecting the shear effect of the beam deflection, the equivalent crack length (a) is derived as

$$a=\left(\frac{3}{2}EIC\right)^{\frac{1}{3}}, \tag{2}$$

where $C=\delta/P$ is the compliance. Therefore, the crack length can be calculated using the gradient of load–displacement (P–δ) curve for each cycle in the fatigue DCB tests.

For composites and adhesive joints, the FCG rate (da/dN) calculated using raw data fluctuates significantly. Therefore, two methods have been proposed to calculate the FCG rate with reduced data scattering: incremental polynomial method and power-law fitting.[7] For small FCG rates, the power-law fitting approach has a significantly lower variance than that for the incremental polynomial method.[52] Therefore, herein, the power-law fitting was implemented; it is expressed as

$$a=c_1N^{c_2}+c_3, \tag{3}$$

where c_1, c_2, and c_3 are fitting parameters. Differentiating Equation (3), the FCG rate is obtained as

$$\frac{da}{dN}=c_1c_2N^{c_2-1}. \tag{4}$$

2.2 | FCG relationship

Originally, the FCG relationship was discussed in metals[53]; moreover, the stress intensity factor range ($\Delta K=K_{\max}-K_{\min}$) is considered as a crack driving force (CDF). Conversely, calculating the stress intensity factor K around the crack tip of inhomogeneous materials such as adhesive layer is significantly complex. Because it is known that the stress intensity factor and SERR have direct relation, the SERR obtained from the DCB tests is more generally used instead of the stress intensity factor for composites and adhesive joints, and $G_{\max}$ and ΔG are most commonly used as CDFs in literature, where $G_{\max}$ is the maximum value of the SERR given as

$$G_{\max}=\frac{P_{\max}^2a^2}{bEI}, \tag{5}$$

ΔG is the range of the SERR given as

$$\Delta G=G_{\max}-G_{\min}=\left(P_{\max}^2-P_{\min}^2\right)\frac{a^2}{bEI}, \tag{6}$$

and $P_{\max}$ and $P_{\min}$ are the maximum and minimum loads in a cycle, respectively. Therefore, the FCG rate is expressed in the form of the Paris crack growth equation as

$$\frac{da}{dN}=cG_{\max}^m \tag{7}$$

or

$$\frac{\mathrm{da}}{\mathrm{dN}}=\mathrm{c}\Delta\mathrm{G}^{\mathrm{m}}, \tag{8}$$

where c and m are empirical constants. The use of ΔG is analogous to the use of ΔK. Nevertheless, it has been suggested that both of them lead to misleading results for varying R-ratio.[54–56] Based on the similitude hypothesis for metals, the value of da/dN should be greater for higher R-ratio at the same ΔK value; essentially, the FCG relationship moves to the upper left as the R-ratio increases. However, several studies have reported the opposite trend while using $G_{\max}$ or ΔG.[14,19,57] Because of the relationship $K\propto\sqrt{G}$ between the stress intensity factor and SERR, the physical implications of using the square root of SERR have been investigated.[54,55,58,59] Moreover, it has been reported that to correctly apply the similarity principle with regards to ΔK, the appropriate expression of CDF is neither $G_{\max}$ nor ΔG, but rather

$$G_{\Delta P}=\left(\sqrt{G_{\max}}-\sqrt{G_{\min}}\right)^2=\frac{\Delta P^2a^2}{bEI}, \tag{9}$$

where $\Delta P=P_{\max}-P_{\min}$ is the range of load in a cycle. Because $G_{\Delta P}$ is proportional to $(\Delta P)^2$, $\Delta K\propto\sqrt{G_{\Delta P}}$ maintained, and the Paris crack growth equation is given as

$$\frac{da}{dN} = cG_{\Delta P}^{m}. \tag{10}$$

For load-controlled fatigue tests, R-ratio is represented as $R = P_{\min}/P_{\max}$. Therefore, $G_{\min}/G_{\max}$ is proportional to R^2, and Equations (8) and (9) can be re-expressed as

$$\Delta G = G_{\max}\left(1 - R^2\right) \tag{11}$$

and

$$G_{\Delta P} = G_{\max}(1 - R)^2, \tag{12}$$

respectively. Equations (11) and (12) cannot be derived theoretically for displacement-controlled fatigue tests, but if linearity in the load–displacement relation is maintained, $\delta_{\min}/\delta_{\max} \approx P_{\min}/P_{\max}$ stands. Therefore, Equations (11) and (12) approximately hold in such cases.

3 | EXPERIMENTAL SETUP

3.1 | Specimen preparation

Figure 1 shows the double cantilever beam specimen that is used for the tests. First, the surfaces of carbon steel (S50C) substrates were sandblasted with alumina grit and wiped with acetone prior to bonding. The adhesive thickness was adjusted to 0.15 ± 0.01 mm by inserting polytetrafluoroethylene (PTFE) tape at the front and back of the adhesive layer. Finally, the substrates were bonded with a second-generation acrylic adhesive for structural use (Hardloc C355-20A/B. Denka Co., Ltd., Tokyo, Japan).

3.2 | Fatigue tests

All fatigue DCB tests were performed under displacement control at a cyclic frequency of 10 Hz using a servo-hydraulic fatigue testing machine (8800 series, Instron Japan Co., Ltd, Kanagawa, Japan). The testing environment had a temperature of $23 \pm 2°C$ and relative humidity lower than 60%. First, the R-ratio was varied while maintaining the mean displacement $\delta_{\text{mean}} = (\delta_{\max} + \delta_{\min})/2$ or the maximum displacement $\delta_{\max}$ constant, as shown in Figure 2A and B, respectively. In both cases, the peak-to-peak amplitude $\Delta\delta = \delta_{\max} - \delta_{\min}$ decreases with increasing R. In addition, the stress waveform parameters were varied while maintaining $\Delta\delta$ or R constant, as shown in Figure 2C and D, respectively. The fatigue tests were completed after 10^7 cycles, followed by static fracture tests to measure the mode I critical fracture energy G_{IC}. The static fracture tests were conducted for normalizing the SERRs obtained in the fatigue tests.

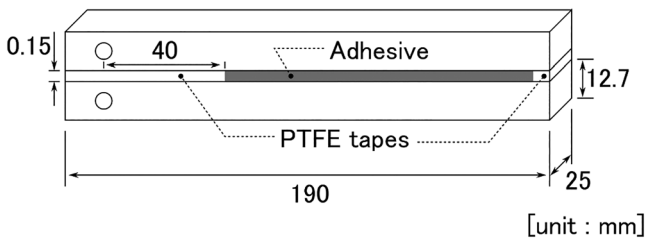

FIGURE 1 DCB specimen geometry. DCB, double cantilever beam, PTFE, polytetrafluoroethylene

4 | RESULTS AND DISCUSSION

Fractured surfaces of some samples were shown in Figure 3. From the macroscopic observation, fatigue failure was considered cohesive for all the tested specimens. Microscopic surface analysis was not performed in this study, but detailed surface analysis using scanning electron microscopy (SEM) revealed that there were hackles and striations in the case of fatigue delamination of composite structures.[40] It was discussed in relation to the change in fracture mechanism due to monotonic and cyclic load, and a multi-parametric FCG relationship was proposed.[41] Although the fracture mechanism changes if the type of plastics changes, further research focusing on a microscopic point of view is expected as it may lead to a more detailed understanding of the fatigue fracture mechanism of this type of adhesive. In order to check the frequency effect, 1 and 10 Hz results were compared in the case of $R = 0.2$ and $\delta_{\text{mean}} = 0.30$ mm, and it was verified that there was no considerable difference in the range of the tested frequency, as shown in Figure 4.

Figure 5A–C and D–F show the FCG relationships of $G_{\max}$, ΔG, and $G_{\Delta P}$ for constant δ_{mean} and $\delta_{\max}$, respectively. From Equations (11) and (12), note that $G_{\max} > \Delta G > G_{\Delta P}$ for $0 < R < 1$. In addition, the higher the R, the larger the gap between $G_{\max}$, ΔG, and $G_{\Delta P}$. Thus, for $G_{\Delta P}$, the overlap was eliminated, the results were aligned in the order of R, and the similitude hypothesis was confirmed.

Focusing on the slope of FCG relationships, the change was observed according to the loading conditions. Therefore, the results were classified into the following three types, as shown in Figure 6. Type I: the slope of the log–log FCG relationship is gentle and almost constant for the entire range; type II: the slope changes from steep to gentle in the middle; and type III: the slope is steep for

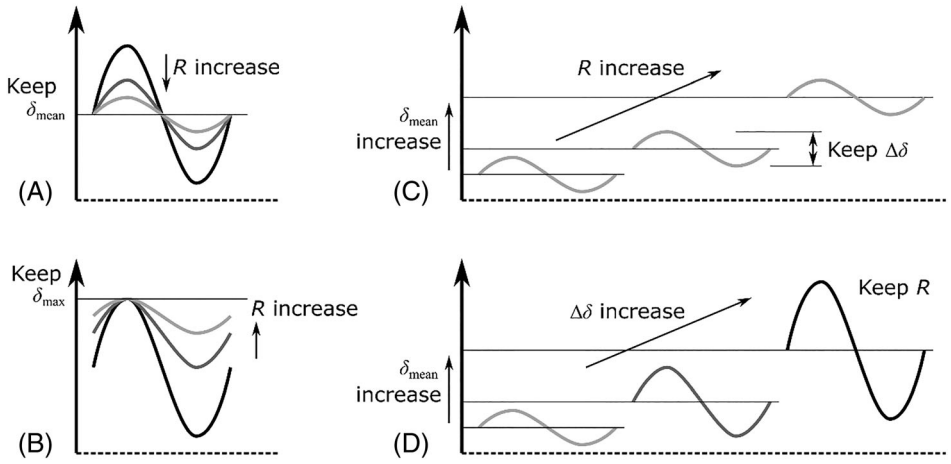

FIGURE 2 Schematics of displacement waveform while (A) δ_{mean}, (B) δ_{max}, (C) $\Delta\delta$, and (D) R are kept constant

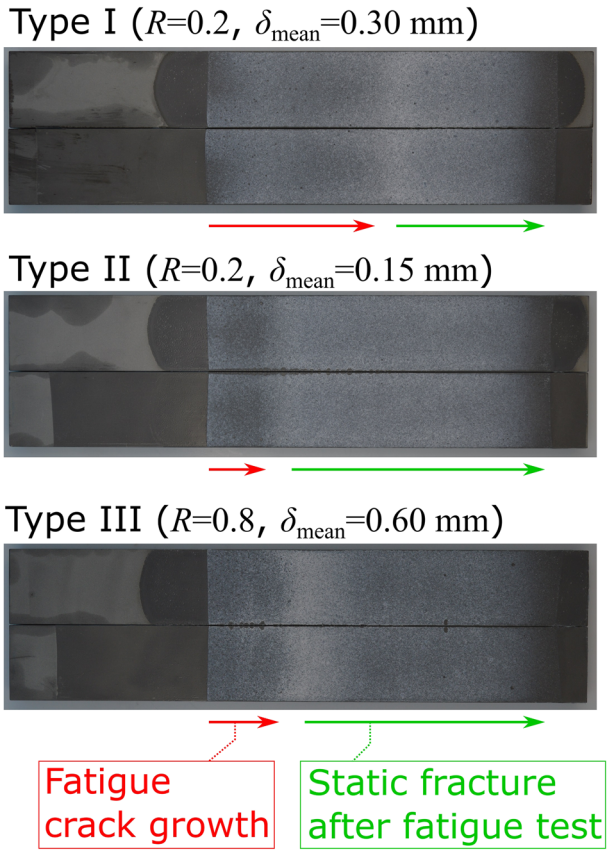

FIGURE 3 Fractured surfaces after the fatigue and quasi-static tests for some cases [Colour figure can be viewed at wileyonlinelibrary.com]

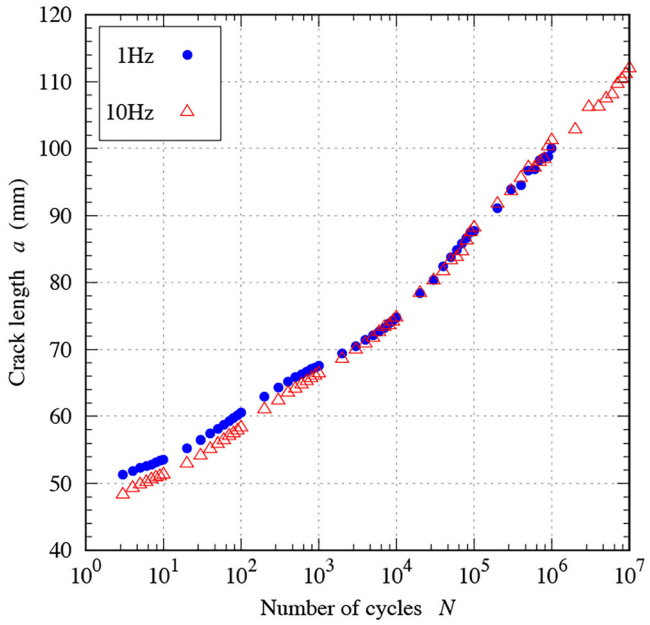

FIGURE 4 Comparison of the results of the crack length versus number of cycles for frequency 1 and 10 Hz in the case of $R = 0.2$ and $\delta_{mean} = 0.30$ mm [Colour figure can be viewed at wileyonlinelibrary.com]

the entire range. Note that classification criteria are necessary to determine the types. Therefore, herein, the boundary between the steep and gentle slopes was given as $m = 10$. Tables 1 and 2 list the slope m in the range of two FCG rates. For the constant δ_{mean}, $R = 0.1$ and 0.2 were classified as type I, 0.5 as type II, and 0.8 and 0.9 as type III, respectively. For the constant δ_{max}, $R = 0.1$, 0.2, and 0.5 were classified as type I, and 0.8 and 0.9 as type III. The slope m in the gentle slope region was approximately 5 to 7 in most cases regardless of the SERR expression, which is reasonable to be considered the FCG belongs to a Paris law region according to that of other adhesive results.[10,22,27,56] Thus, fatigue dominant crack growth occurred under the gentle slope region. Conversely, when the slope was steep, the slope m changed depending on the SERR expression. In addition, comparing the position of the FCG relationship of $G_{\Delta P}$, the steep slope region made a bigger difference depending on the loading condition than the gentle slope region. Because a steeper slope corresponds to a delay in crack growth for displacement-controlled fatigue tests, a crack after

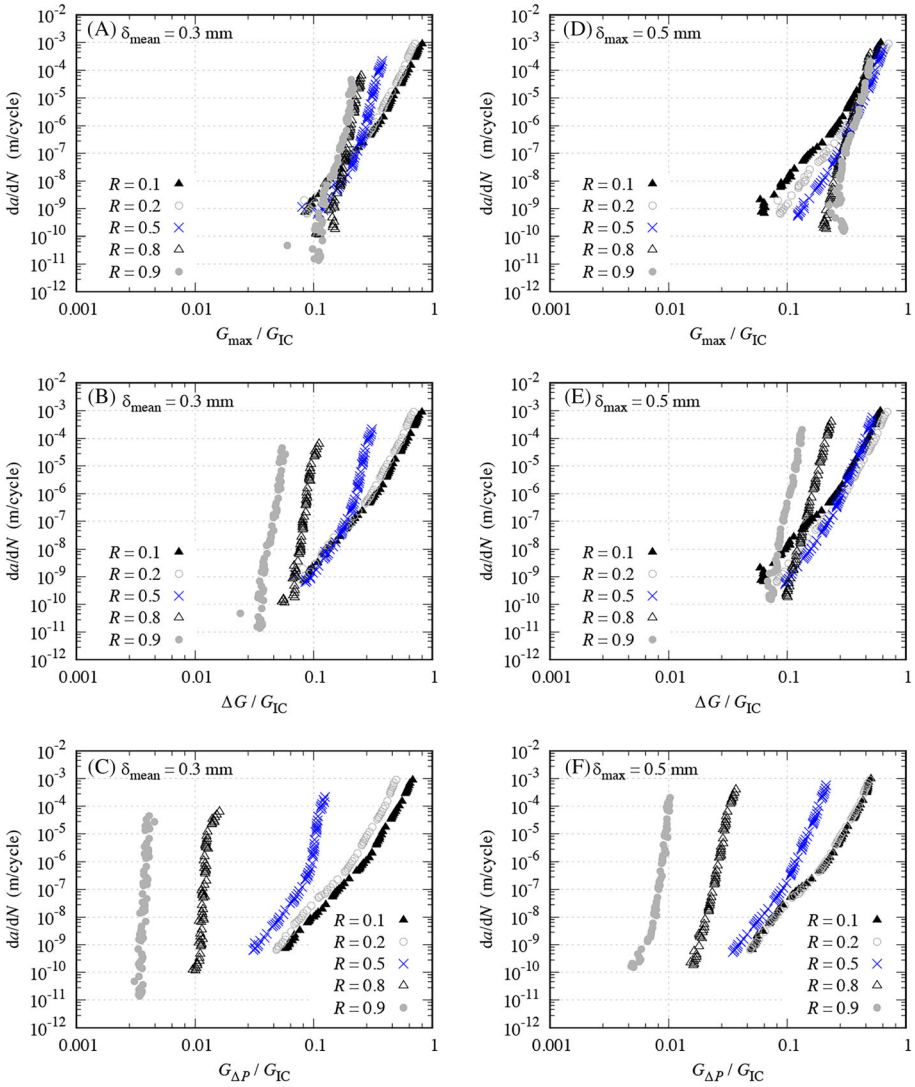

FIGURE 5 FCG relationship of G_{max}, ΔG, and $G_{\Delta P}$ for (A–C) constant δ_{mean} and (D–F) constant δ_{max}. FCG, fatigue crack growth [Colour figure can be viewed at wileyonlinelibrary.com]

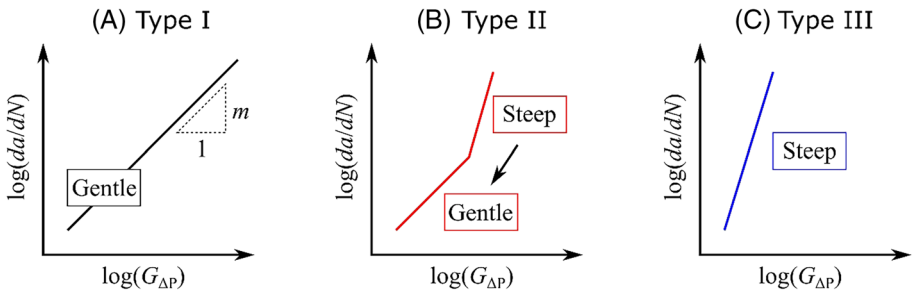

FIGURE 6 Schematics for types of the FCG relationship due to the difference in slope. FCG, fatigue crack growth [Colour figure can be viewed at wileyonlinelibrary.com]

10^7 cycles was shorter with larger R, as shown in Figure 7. Prediction of the amount of FCG is industrially important, and it is necessary to clarify which parameter has a dominant effect.

Figures 8 and 9 show the FCG relationships of $G_{\Delta P}$ and a–N curves for constant $\Delta\delta$ and constant R, respectively. When $\Delta\delta$ was constant, the crack propagated more for a larger R. This trend is the opposite of that observed when the mean or max displacement is maintained constant. Therefore, it became clear that a smaller R does not always mean more crack propagation. The difference in crack position after 10^7 cycles for constant $\Delta\delta$ was not as significant as when the other parameters were changed, as shown in Figure 8D–F. In addition, the larger $\Delta\delta$, the more the crack propagated after a sufficient number of fatigue cycles. Therefore, the crack position was strongly

TABLE 1 Gradient of the slope m obtained by varying R while $\delta_{mean} = 0.30$ mm

R	Range of fitting	m for G_{max}	m for ΔG	m for $G_{\Delta P}$
0.1	$10^{-6} \le da/dN \le 10^{-4}$	7.86	7.82	7.37
	$10^{-9} \le da/dN \le 10^{-7}$	5.09	5.02	4.64
0.2	$10^{-6} \le da/dN \le 10^{-4}$	7.80	7.72	7.16
	$10^{-9} \le da/dN \le 10^{-7}$	5.11	5.04	4.76
0.5	$10^{-6} \le da/dN \le 10^{-4}$	17.7	19.7	26.0
	$10^{-9} \le da/dN \le 10^{-7}$	6.47	6.13	5.45
0.8	$10^{-6} \le da/dN \le 10^{-4}$	20.7	17.3	14.0
	$10^{-9} \le da/dN \le 10^{-7}$	17.7	27.0	91.1
0.9	$10^{-6} \le da/dN \le 10^{-4}$	32.9	45.8	83.7
	$10^{-9} \le da/dN \le 10^{-7}$	12.0	18.8	54.3

TABLE 2 Gradient of the slope m obtained by varying R while $\delta_{max} = 0.50$ mm

R	Range of fitting	m for G_{max}	m for ΔG	m for $G_{\Delta P}$
0.1	$10^{-6} \le da/dN \le 10^{-4}$	7.40	7.39	7.23
	$10^{-9} \le da/dN \le 10^{-7}$	4.79	4.81	5.09
0.2	$10^{-6} \le da/dN \le 10^{-4}$	7.80	7.72	7.16
	$10^{-9} \le da/dN \le 10^{-7}$	5.11	5.04	4.76
0.5	$10^{-6} \le da/dN \le 10^{-4}$	9.56	9.66	9.85
	$10^{-9} \le da/dN \le 10^{-7}$	6.49	6.11	5.40
0.8	$10^{-6} \le da/dN \le 10^{-4}$	14.2	17.5	26.7
	$10^{-9} \le da/dN \le 10^{-7}$	16.7	16.3	15.6
0.9	$10^{-6} \le da/dN \le 10^{-4}$	17.0	23.7	44.4
	$10^{-9} \le da/dN \le 10^{-7}$	36.6	27.4	21.3

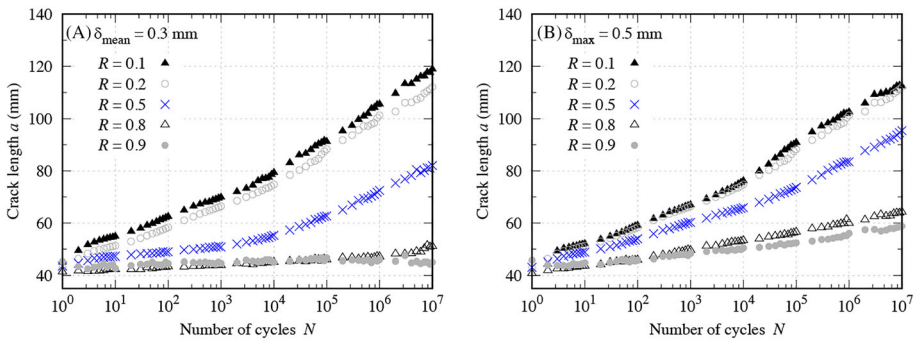

FIGURE 7 Crack length versus number of cycles (a–N) curves for (A) constant δ_{mean} and (B) constant δ_{max} [Colour figure can be viewed at wileyonlinelibrary.com]

dominated by $\Delta\delta$ in high cycle fatigue. Figure 10 shows the crack position after 10^7 cycles against R, δ_{mean}, and $\Delta\delta$. It also clearly indicated the dependency of the amount of FCG on $\Delta\delta$.

Discussion of FCG using SERR or stress intensity factor is based on empirical analysis. Therefore, a new approach based on a physical point of view has been introduced.[60–63] Strain energy in the specimen is calculated from the force and the displacement as[62]

$$U_{tot} = \frac{1}{2} P_{max} (\delta_{max} - \delta_0), \tag{13}$$

where $\delta_0 = \delta_{max} - CP_{max}$. Originally, the relation between U_{tot} and N was fitted using a power law,[60] and the results obtained here did not fit well. Therefore,

$$U_{tot} = d_1 \log N + d_2 \tag{14}$$

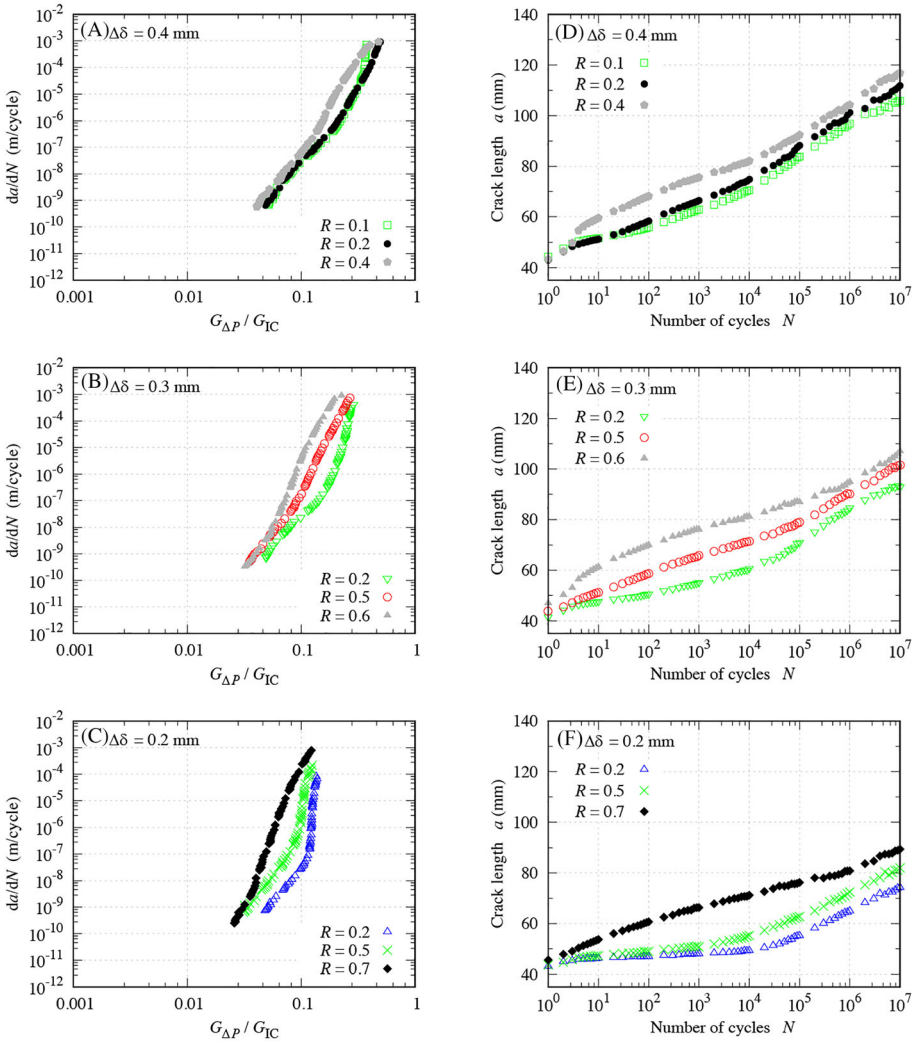

FIGURE 8 FCG relationship and crack length versus number of cycles (a–N) curves for constant amplitude with (A and D) $\Delta\delta = 0.4$ mm, (B and E) $\Delta\delta = 0.3$ mm, and (C and F) $\Delta\delta = 0.2$ mm. FCG, fatigue crack growth [Colour figure can be viewed at wileyonlinelibrary.com]

was used for fitting, where d_1 and d_2 are fitting parameters. Similar to the Paris crack growth equation, the relation between the FCG rate da/dN and the loss of total strain energy per cycle $-dU_{\text{tot}}/dN$ can be captured by a power-law relationship as

$$\frac{da}{dN} = k\left(-\frac{dU_{\text{tot}}}{dN}\right)^n, \tag{15}$$

where k and n are the fitting parameters. Seven-point incremental polynomial method[64] was also used for the derivation of da/dN and $-dU_{\text{tot}}/dN$. Three results from each type ($R = 0.2$ and $\delta_{\text{mean}} = 0.15$ mm, $R = 0.2$ and $\delta_{\text{mean}} = 0.30$ mm, and $R = 0.8$ and $\delta_{\text{mean}} = 0.30$ mm) were compared, as shown in Figure 11. Here, the condition $R = 0.2$ and $\delta_{\text{mean}} = 0.15$ mm is related to type II. From the FCG rate change against number of cycles as shown in Figure 11C, it was revealed that types I and III kept the gap almost constant in a double logarithmic graph. In the case of type II, it was close to the type III rate at first, but with increasing the number of cycles, it got close to the type I rate. The same trend was observed in the slope change of the FCG relationship of $G_{\Delta P}$, as shown in Figure 11E. Therefore, it was speculated that the change in the FCG rate and the change in the slope of the FCG relationship of $G_{\Delta P}$ were related. Conversely, no trend change in the middle of the test was confirmed in U_{tot} or $-dU_{\text{tot}}/dN$ for type II, although the results of da/dN versus $-dU_{\text{tot}}/dN$ were almost in a single line regardless of the loading conditions, as shown in Figure 11F, which was the same trend as previously reported.[60–62] Because da/dN and $-dU_{\text{tot}}/dN$ expresses crack initiation and energy change at the cycle number N, another expression for the SERR can be obtained by dividing $-dU_{\text{tot}}/dN$ by da/dN as[61]

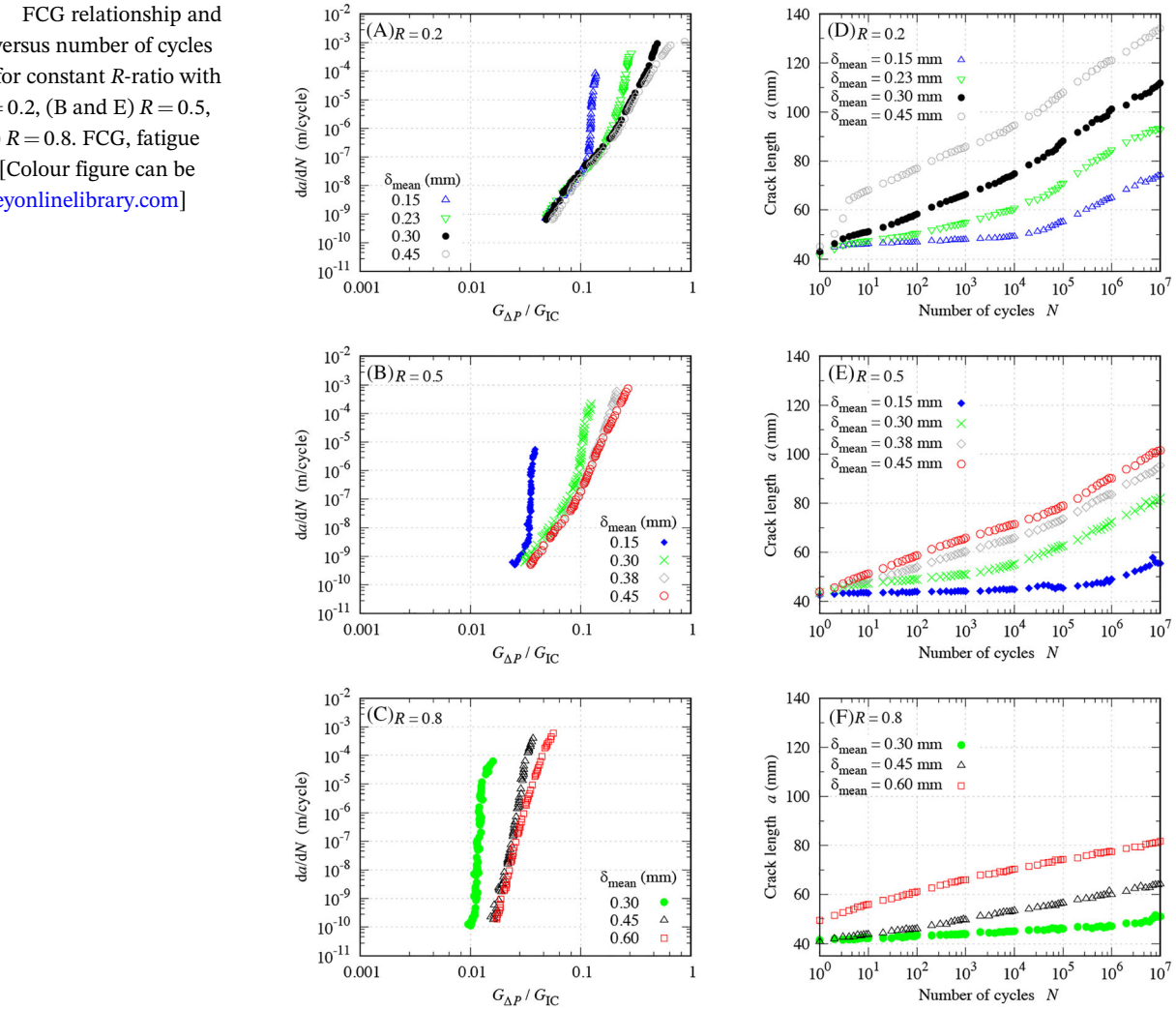

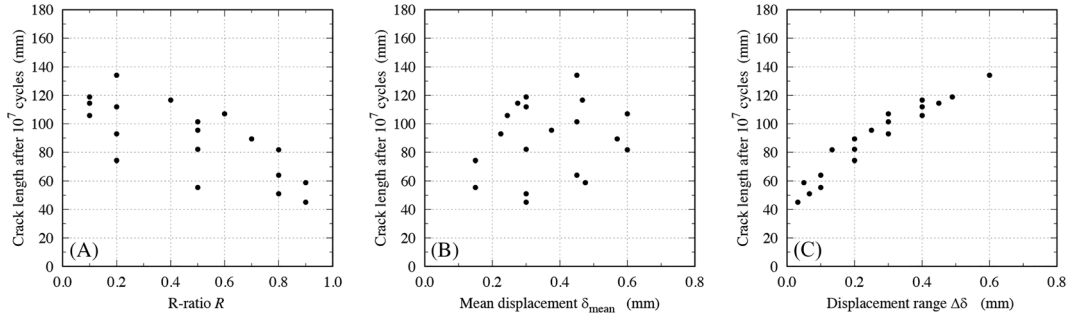

FIGURE 9 FCG relationship and crack length versus number of cycles (a–N) curves for constant R-ratio with (A and D) $R = 0.2$, (B and E) $R = 0.5$, and (C and F) $R = 0.8$. FCG, fatigue crack growth [Colour figure can be viewed at wileyonlinelibrary.com]

FIGURE 10 The crack length after 10^7 cycles in relation to (A) R-ratio, (B) mean displacement, and (C) displacement range

$$G^* = \frac{-\frac{dU_{\text{tot}}}{dN}}{\frac{da}{dN} \cdot b}. \tag{16}$$

It can be understood as the average amount of the strain energy released per unit crack length during cycle number N. The results for each type are shown in Figure 12.

Excluding variation, G^* ranged roughly from 10^2 to 10^3 J/m^2, which was closed to the value of $G_{\max}$. It might be because both G^* and $G_{\max}$ were calculated from the maximum load. In the case of type I, G^* was almost constant, whereas $G_{\Delta P}$ and $G_{\max}$ gradually decreased. In the case of type II, a decrease in SERR was observed after a sufficient number of cycles, regardless of the SERR expression. In the case of type III, the values of SERRs were less

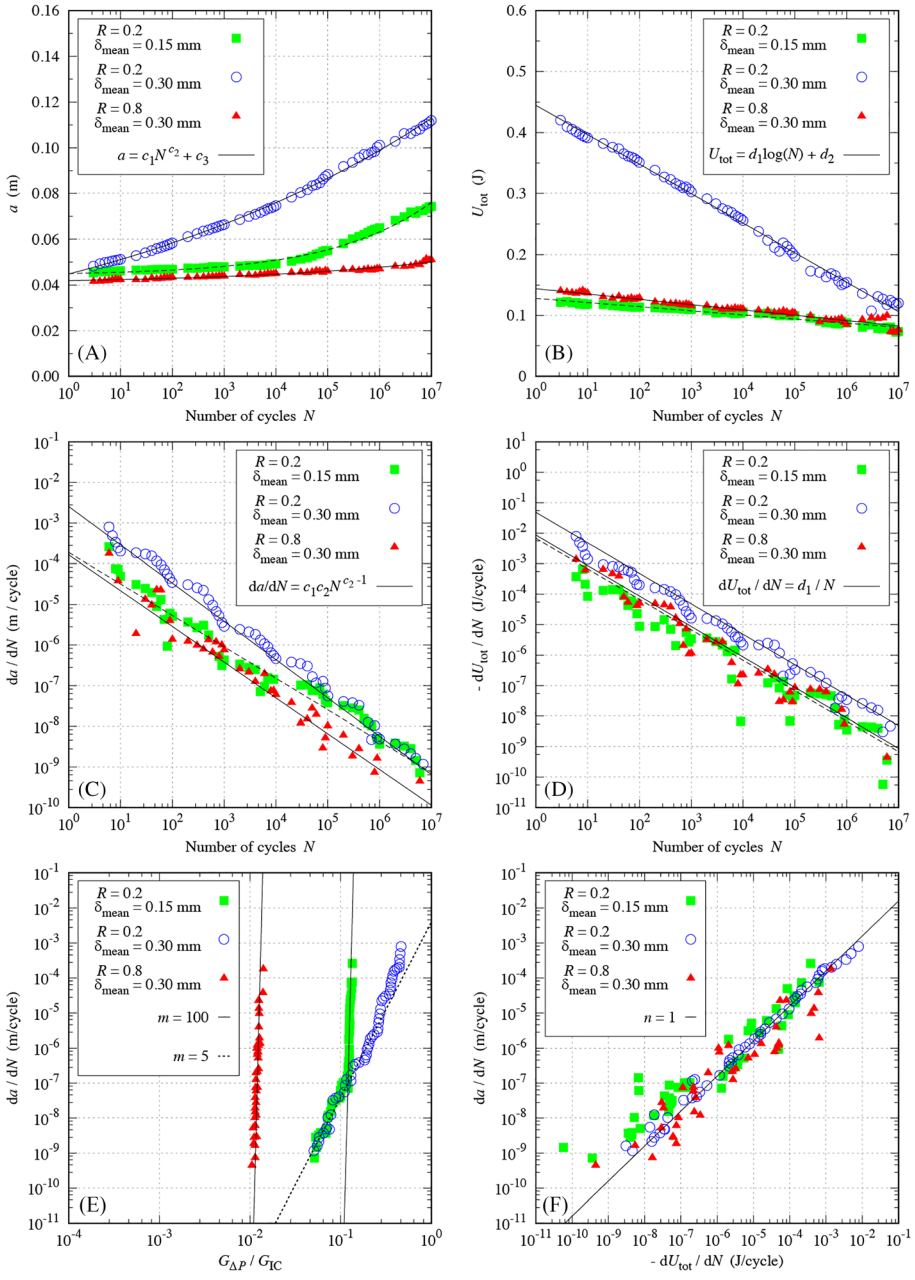

FIGURE 11 The results of selected samples (type I for $R = 0.2$ and $\delta_{mean} = 0.30$ mm, type II for $R = 0.2$ and $\delta_{mean} = 0.15$ mm, and type III for $R = 0.8$ and $\delta_{mean} = 0.30$ mm). (A) Crack length versus number of cycles. (B) Total strain energy versus number of cycles. (C) FCG rate versus number of cycles. (D) Loss of total strain energy per cycle versus number of cycles. (E) FCG rate versus normalized equivalent energy release rate range. (F) FCG rate versus loss of total strain energy per cycle. FCG, fatigue crack growth [Colour figure can be viewed at wileyonlinelibrary.com]

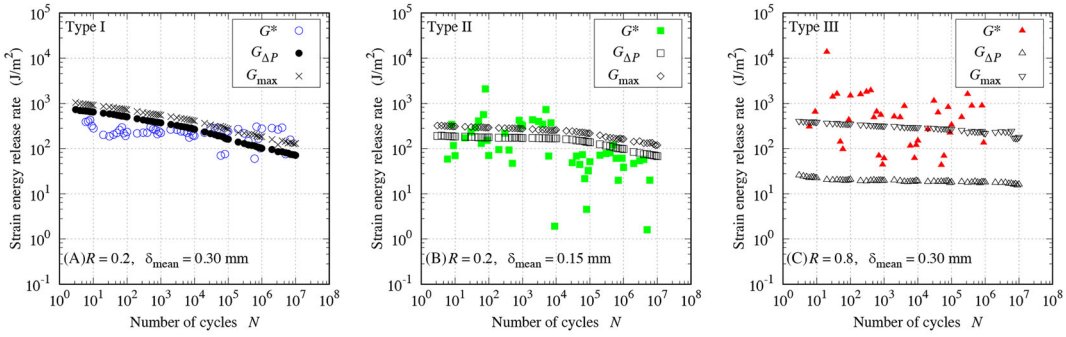

FIGURE 12 The results of strain energy release rate versus the number of cycles. (A) Type I with $R = 0.2$ and $\delta_{mean} = 0.30$ mm, (B) type II with $R = 0.2$ and $\delta_{mean} = 0.15$ mm, and (c) type III with $R = 0.8$ and $\delta_{mean} = 0.30$ mm [Colour figure can be viewed at wileyonlinelibrary.com]

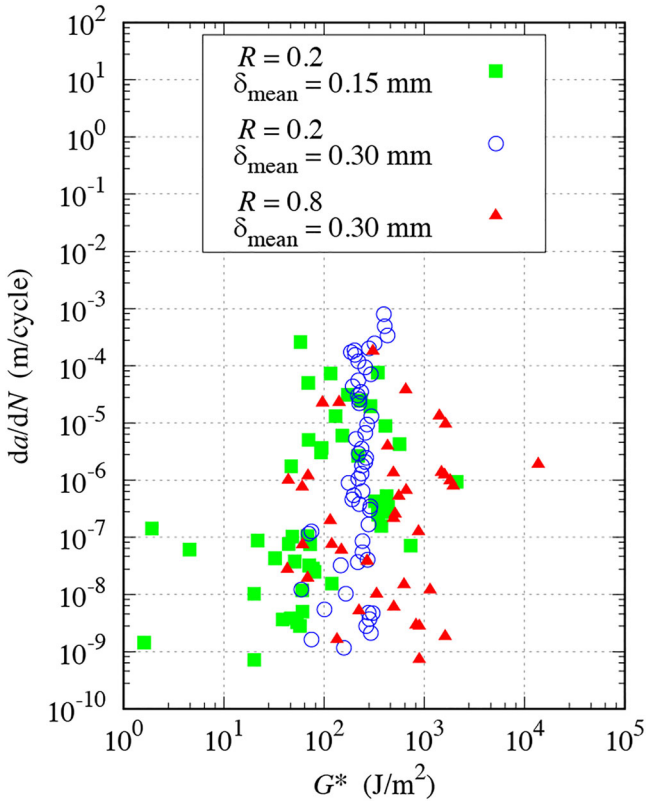

FIGURE 13 FCG relationship of G^* with $(R, \delta_{mean}) = (0.2, 0.30\,mm)$, (0.2, 0.15 mm), and (0.8, 0.30 mm). FCG, fatigue crack growth [Colour figure can be viewed at wileyonlinelibrary.com]

sensitive to the cycle number. The relationship between the FGC rate and the average strain energy release rate is shown in Figure 13. Because of the large deviation of G^*, the change of circumstances was difficult to be detected from the FCG relationship of G^*. However, from Figure 12B, it was indicated that a change in the FCG rate for type II can be possibly detected by the SERR change, regardless of the SERR expression. When δ_{mean} was varied while maintaining R constant, deviation in the FCG relationship before reaching the Paris law region, that is, the steep slope range, was revealed for $R = 0.2$ and 0.5, as shown in Figure 9A and B, respectively. The SERR value in this steep slope region varied depending on the loading condition. In addition, the steep slope was more prominent for smaller δ_{mean}. Therefore, next, the dominant factor to generate the steep slopes was discussed. In the case of composites, changing the mean load while maintaining the R-ratio constant reportedly changes the FCG relationship.[65] Some studies on polymers have suggested that FCG at a high R-ratio is promoted by creep behavior[59,66] and that the magnitude of mean stress alters the FCG speed.[67,68] For adhesive joints, no clear method has been developed to explain the change in FCG behavior due to loading conditions, but the use of mean value is suggested as a reliable option when the creep effect is dominant.[20] In such cases, $(G_{max} + G_{min})/2$ is often used. However, in this study,

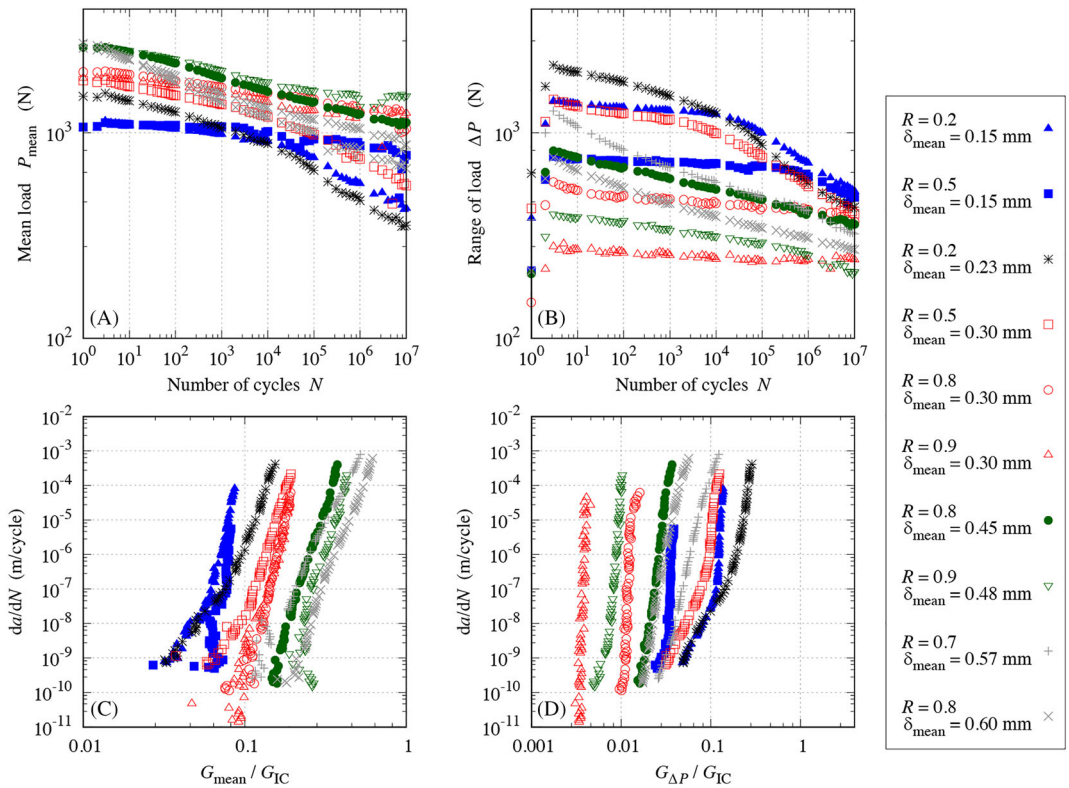

FIGURE 14 (A) Mean load versus number of cycles, (B) range of load versus number of cycles, (C) FCG relationship of G_{mean}, and (D) FCG relationship of $G_{\Delta P}$. FCG, fatigue crack growth [Colour figure can be viewed at wileyonlinelibrary.com]

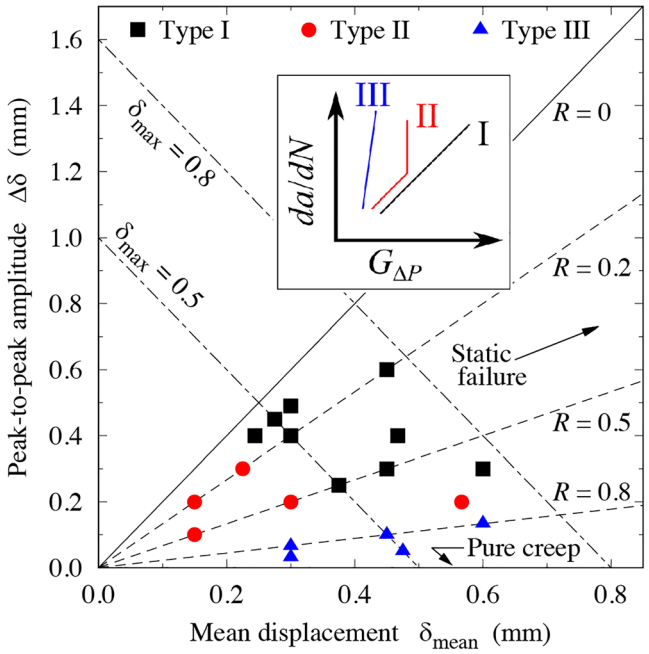

FIGURE 15 Peak-to-peak amplitude versus mean displacement plot to classify the FCG behavior into type I (ΔP dominance), type II (P_{mean} to ΔP dominance), and type III (P_{mean} dominance). FCG, fatigue crack growth [Colour figure can be viewed at wileyonlinelibrary.com]

the following was adopted with reference to the similitude of $G_{\Delta P}$.

$$G_{mean} = \frac{P_{mean}^2 a^2}{bEI}, \tag{16}$$

where $P_{mean} = (P_{max} + P_{min})/2$. $G_{\Delta P}$ is proportional to $(\Delta P)^2$ and the similitude to ΔK is confirmed. Because G_{mean} is proportional to $(P_{mean})^2$, the similitude to the mean stress intensity factor $K_{mean} = (K_{max} + K_{min})/2$ is expected. The results of types II and III are plotted together while comparing ΔP and P_{mean} results, as shown in Figure 14. The results were color-coded by the mean displacement. In most cases, P_{mean} values were larger with larger δ_{mean} in the small N range, but the regularity disappeared as N increased. ΔP had no regularity in the mean displacement but converged overall with increasing N. Similar to P_{mean} change, the FCG relationships of G_{mean} in the steep slope region were almost aligned in the order of the mean displacement. The smaller the δ_{mean}, the more the FCG relation shifted toward left. Conversely, the FCG relationships of $G_{\Delta P}$ were inconsistent with respect to the mean displacement. Thus, it was indicated that slow crack growth was affected by the mean value, and creep dominant crack growth occurred under the steep slope region.

Figure 15 shows the amplitude versus mean displacement plot, which classifies the FCG types. In the quasi-static tests, the crack started propagating at $\delta \approx 0.8$. Therefore, on the upper right side of the $\delta_{max} = 0.8$ line, the crack may rapidly propagate in a few load cycles. $\Delta\delta = 0$ means pure creep condition. Therefore, type III results were positioned at the bottom. In contrast, types I and II results tended to gather in the upper half and middle of a triangle surrounded by the $\delta_{max} = 0.8$ line and the $R = 0$ line, respectively. Pure FCG (type I) appeared only in a significantly narrow range of loading conditions with high loading levels, revealing that the amplitude is more important than the R-ratio. In addition, the type II conditions need to be dealt with carefully because the crack may propagate at an accelerated rate in further load cycles even if the cracks do not appear to be growing at first.

5 | CONCLUSION

FCG behavior of a structural acrylic adhesive was investigated by varying the parameters related to the shape of a sinusoidal wave produced during the displacement-controlled fatigue DCB tests with a frequency of 10 Hz. First, the difference of the fracture energy expression according to the R-ratio was investigated, and a trend similar to the one traditionally reported for epoxy adhesives was obtained. Essentially, $G_{\Delta P} = \left(\sqrt{G_{max}} - \sqrt{G_{min}}\right)^2$ showed consistency with the similitude hypothesis. Comparing the effect of R-ratio, mean displacement, and amplitude on the amount of crack growth in a high cycle fatigue regime, the amplitude had the most consistent relationship to the crack position. Therefore, reducing the amplitude is the key to suppressing crack growth. Under some loading conditions, the trend of FCG rate variation changed in the middle of the fatigue tests. In such cases, variation of SERR in the middle was also confirmed, and it was considered the driving force for crack propagation acceleration. Amplitude versus mean displacement diagram was introduced to classify changes in FCG trends. Complex phenomena involving fatigue and creep may be peculiar to ductile adhesives such as SGAs, but in other words, it was revealed that the FCG behavior is highly related to the type of adhesive. Therefore, it will be undoubtedly important to have a deeper understanding of the FCG behavior of various adhesive types as the demand for adhesive joints increases.

ACKNOWLEDGMENTS

We would like to thank Editage (www.editage.com) for English language editing.

FUNDING INFORMATION

This work was funded by the New Energy and Industrial Technology Development Organization (NEDO) under Project Number JPNP14014.

CONFLICTS OF INTEREST

The authors declare that there are no conflicts of financial interest or personal relationships that can inappropriately influence the work reported in this paper.

DATA AVAILABILITY STATEMENT

The data that support the findings of this study are available from the corresponding author upon reasonable request.

NOMENCLATURE

a	crack length
b	width of substrate
c	constant in the Paris crack growth equation
c_1,c_2,c_3	curve fit parameters
C	compliance
d_1,d_2	curve fit parameters
E	Young's modulus of substrate
G	strain energy release rate, fracture energy
G^*	average strain energy release rate
$G_{\max}$, $G_{\min}$, G_{mean}	strain energy release rate at maximum, minimum, and mean loads in a fatigue cycle
$G_{\Delta P}$	equivalent energy release rate range
G_{IC}	mode I critical energy release rate
I	moment of inertia of substrate cross-section
k	constant in the strain energy-based crack growth equation
K	stress intensity factor
$K_{\max}$,$K_{\min}$,K_{mean}	stress intensity factor at maximum, minimum, and mean loads in a fatigue cycle
m	exponent in the Paris crack growth equation
n	exponent in the strain energy-based crack growth equation
N	number of fatigue cycles
P	load
$P_{\max}$, $P_{\min}$, P_{mean}	maximum, minimum, and mean loads in a fatigue cycle
R	R-ratio (load ratio or displacement ratio)
U_{tot}	total strain energy in a system
δ	displacement
$\delta_{\max}$, $\delta_{\min}$, δ_{mean}	maximum, minimum, and mean displacement in a fatigue cycle
δ_0	displacement for which the force is 0
Δ	crack length correction
ΔG	strain energy release rate range in a fatigue cycle
ΔK	stress intensity factor range
ΔP	load range
$\Delta\delta$	displacement range, peak-to-peak amplitude

ORCID

Yu Sekiguchi https://orcid.org/0000-0003-3290-7021

REFERENCES

1. ASTM D3166-99. Standard test method for fatigue properties of adhesives in shear by tension loading (Metal/Metal). American Society for Testing Materials; 2020.
2. ISO 9664. Adhesives–test methods for fatigue properties of structural adhesives in tensile shear. International Organization for Standardization; 1993.
3. ASTM D6115-97. Standard test method for mode I fatigue delamination growth onset of unidirectional fiber-reinforced polymer matrix composites. American Society for Testing Materials; 2019.
4. Murri GB. Effect of data reduction and fiber-bridging on mode I delamination characterization of unidirectional composites. *J Thermoplast Compos Mater*. 2014;48(19):2413-2424.
5. Brunner AJ, Murphy N, Pinter G. Development of a standardized procedure for the characterization of interlaminar delamination propagation in advanced composited under fatigue mode I loading conditions. *Eng Fract Mech*. 2009;76(18):2678-2689.
6. Stelzer S, Brunner AJ, Argüelles A, Murphy N, Pinter G. Mode I delamination fatigue crack growth in unidirectional fiber reinforced composites: development of a standardized test procedure. *Compos Sci Technol*. 2012;72(10):1102-1107.
7. Stelzer S, Brunner AJ, Argüelles A, Murphy N, Cano GM, Pinter G. Mode I delamination fatigue crack growth in unidirectional fiber reinforced composites: results from ESIS TC4 round-robins. *Eng Fract Mech*. 2014;116:92-107.
8. Brunner AJ, Stelzer S, Pinter G, Terrasi GP. Cyclic fatigue delamination of carbon fiber-reinforced polymer-matrix composites: data analysis and design considerations. *Int J Fatigue*. 2016;83:293-299.
9. Mall S, Ramamurthy G. Effect of bond thickness on fracture and fatigue strength of adhesively bonded composite joints. *Int J Adhes Adhes*. 1989;9(1):33-37.
10. Kinloch AJ, Osiyemi SO. Predicting the fatigue life of adhesively bonded joints. *J Adhes*. 1993;43(1-2):79-90.
11. Jethwa JK, Kinloch AJ. The fatigue and durability behaviour of automotive adhesives. Part I: fracture mechanics tests. *J Adhes*. 1997;61(1-4):71-95.
12. Kinloch AJ, Little MSG, Watts JF. The role of the interphase in the environmental failure of adhesive joints. *Acta Mater*. 2000;48(18–19):4543-4553. doi:10.1016/S1359-6454(00)00240-8

13. Hadavinia H, Kinloch AJ, Little MSG, Taylor AC. The prediction of crack growth in bonded joints under cyclic-fatigue loading I. Experimental studies. *Int J Adhes Adhes*. 2003;23(6):449-461.
14. Erpolat S, Ashcroft IA, Crocombe AD, Abdel-Wahab MM. Fatigue crack growth acceleration due to intermittent overstressing in adhesively bonded CFRP joints. *Compos A*. 2004;35(10):1175-1183.
15. Abel ML, Adams ANN, Kinloch AJ, Shaw SJ, Watts JF. The effects of surface pretreatment on the cyclic-fatigue characteristics of bonded aluminium-alloy joints. *Int J Adhes Adhes*. 2006;26(1–2):50-61.
16. Fernández MV, de Moura MFSF, da Silva LFM, Marques AT. Composite bonded joints under mode I fatigue loading. *Int J Adhes Adhes*. 2011;31(5):280-285.
17. Azari S, Ameli A, Datla NV, Papini M, Spelt JK. Effect of substrate modulus on the fatigue behavior of adhesively bonded joints. *Mater Sci Eng A*. 2012;534:594-602.
18. Datla NV, Ameli A, Azari S, Papini M, Spelt JK. Effect of hygrothermal aging on the fatigue behavior of two toughened epoxy adhesives. *Eng Fract Mech*. 2012;79:61-77.
19. Shahverdi M, Vassilopoulos AP, Keller T. Experimental investigation of R-ratio effects on fatigue crack growth of adhesively-bonded pultruded GFRP DCB joints under CA loading. *Compos A*. 2012;43(10):1689-1697.
20. Azari S, Jhin G, Papini M, Spelt JK. Fatigue threshold and crack growth rate of adhesively bonded joints as a function of load/displacement ratio. *Compos a*. 2014;57:59-66.
21. Costa M, Viana G, da Silva LFM, Campilho RDSG. Effect of humidity on the fatigue behaviour of adhesively bonded aluminium joints. *Latin Am J Solids Struct*. 2017;14(1):174-187.
22. Rocha AVM, Akhavan-Safar A, Carbas R, et al. Paris law relations for an epoxy-based adhesive. *Proc Inst Mech Eng Pt L: J Mater Design Appl*. 2020;234(2):291-299.
23. Pascoe JA, Zavatta N, Troiani E, Alderliesten RC. The effect of bond-line thickness on fatigue crack growth rate in adhesively bonded joints. *Eng Fract Mech*. 2020;229:106959.
24. Villamil AAB, Rodriguez JPC, Holguin AP, Barrera MS. Mode I crack propagation experimental analysis of adhesive bonded joints comprising glass fibre composite material under impact and constant amplitude fatigue loading. *Materials*. 2021;14(16):4380.
25. Bello I, Alowayed Y, Albinmousa J, Lubineau G, Merah N. Fatigue crack growth in laser-treated adhesively bonded composite joints: An experimental examination. *Int J Adhes Adhes*. 2021;105:102784.
26. Sekiguchi Y, Yamagata Y, Sato C. Mode I fracture energy of adhesive joints bonded with adhesives with different characteristics under quasi-static and impact loading. *J Adhes Soc Jpn*. 2017;53(10):330-337.
27. Rocha AVM, Akhavan-Safar A, Carbas R, et al. Fatigue crack growth analysis of different adhesive systems: effects of mode mixity and load level. *Fatigue Fract Eng Mater Struct*. 2020;43(2):330-341.
28. Aronovich DA, Boinovich LB. Structural acrylic adhesives: a critical review. In: Mittal KL, ed. *Progress in Adhesion and Adhesives, Volume 6, Chapter 15*. Weinheim, Germany: Wiley-VCH Verlag GmbH & Co. KGaA; 2021:651-708.
29. Charnock RS. Structural acrylic adhesives for the sheet steel fabrication industries. *Int J Adhes Adhes*. 1985;5(4):201-206.
30. Pucciariello P, Bianchi N, Braglia R, Garbassi F. The morphology of rubber-modified acrylic adhesives. *Int J Adhes Adhes*. 1989;9(2):77-82.
31. Kamiyama K, Mikuni M, Matsumoto T, Matsuda S, Kishi H. Crack growth mechanism on SGA adhesive joints. *Int J Adhes Adhes*. 2020;103:102690.
32. Hayashi A, Sekiguchi Y, Sato C. AFM observation of sea-island structure formed by second generation acrylic adhesive. *J Adhes*. 2021;97(2):155-171.
33. 3M white paper "Acrylic structural adhesives features and recent advancements"; 2022. https://multimedia.3m.com/mws/media/1054052O/acrylic-adhesives-recent-advancements-white-paper.pdf
34. Imanaka M, Ishii K, Hara K, Ikeda T, Kouno Y. Fatigue crack propagation rate of CFRP/aluminum adhesively bonded DCB joints with acrylic and epoxy adhesives. *Int J Adhes Adhes*. 2018;85:149-156.
35. Kim HB, Naito K, Oguma H. Fatigue crack growth properties of a two-part acrylic-based adhesive in an adhesive bonded joint: double cantilever-beam tests under mode I loading. *Int J Fatigue*. 2017;98:286-295.
36. Sekiguchi Y, Sato C. Effect of bond-line thickness on fatigue crack growth of structural acrylic adhesive joints. *Materials*. 2021;14(7):1723.
37. Pirondi A, Nicoletto G. Mixed mode I/II fatigue crack growth in adhesive joints. *Eng Fract Mech*. 2006;73(16):2557-2568.
38. Pirondi A, Nicoletto G. Fatigue crack growth in bonded DCB specimens. *Eng Fract Mech*. 2004;71(4-6):859-871.
39. Sadananda K, Vasudevan AK. Multiple mechanisms controlling fatigue crack growth. *Fatigue Fract Eng Mater Struct*. 2003;26(9):835-845.
40. Khan R, Alderliesten R, Benedictus R. Two-parameter model for delamination growth under mode I fatigue loading (Part A: experimental study). *Compos A*. 2014;65:192-200.
41. Khan R, Alderliesten R, Benedictus R. Two-parameter model for delamination growth under mode I fatigue loading (Part B: model development). *Compos A*. 2014;65:201-210.
42. Khan R, Alderliesten R, Badshah S, Benedictus R. Effect of stress ratio or mean stress on fatigue delamination growth in composites: critical review. *Compos Struct*. 2015;124:214-227.
43. Beber VC, Baumert M, Klapp O, Nagel C. Fatigue failure criteria for structural film adhesive bonded joints with considerations of multiaxiality, mean stress and temperature. *Fatigue Fract Eng Mater Struct*. 2021;44(3):636-650.
44. Maddox SJ. The effect of mean stress on fatigue crack propagation a literature review. *Int J Fract*. 1975;11(3):389-408.
45. Sun F, Blackman BRK. Using digital image correlation to automate the measurement of crack length and fracture energy in the mode I testing of structural adhesive joints. *Eng Fract Mech*. 2021;255:107957.
46. Terasaki N, Fujio Y, Sakata Y, Horiuchi S, Akiyama H. Visualization of crack propagation for assisting double cantilever beam test through mechanoluminescence. *J Adhes*. 2018;94(11):867-879.
47. Williams JG. End corrections for orthotropic DCB specimens. *Compos Sci Technol*. 1989;35(4):367-376.
48. De Moura MFSF, Morais JJL, Dourado N. A new data reduction scheme for mode I wood fracture characterization using

the double cantilever beam test. *Eng Fract Mech*. 2008;75(13): 3852-3865.

49. Sekiguchi Y, Katano M, Sato C. Experimental study of the mode I adhesive fracture energy in DCB specimens bonded with a polyurethane adhesive. *J Adhes*. 2017;93(3):235-255.
50. Sekiguchi Y, Hayashi A, Sato C. Analytical determination of adhesive layer deformation for adhesively bonded double cantilever beam test considering elastic-plastic deformation. *J Adhes*. 2020;96(7):647-664.
51. Sekiguchi Y, Sato C. Experimental investigation of the effects of adhesive thickness on the fracture behavior of structural acrylic adhesive joints under various loading rates. *Int J Adhes Adhes*. 2021;105:102782.
52. Simon I, Banks-Sills L, Fourman V. Mode I delamination propagation and R-ratio effects in woven composite DCB specimens for a multi-directional layup. *Int J Fatigue*. 2017;96:237-251.
53. Paris P, Erdogan F. A critical analysis of crack propagation laws. *J Basic Eng*. 1963;85(4):528-533.
54. Jones R, Kinloch AJ, Hu W. Cyclic-fatigue crack growth in composite and adhesively-bonded structures: the FAA slow crack growth approach to certification and the problem of similitude. *Int J Fatigue*. 2016;88:10-18.
55. Rans C, Alderliesten R, Benedictus R. Misinterpreting the results: how similitude can improve our understanding of fatigue delamination growth. *Compos Sci Technol*. 2011;71(2): 230-238.
56. Jones R, Hu W, Kinloch AJ. A convenient way to represent fatigue crack growth in structural adhesives. *Fatigue Fract Eng Mater Struct*. 2015;38(4):379-391.
57. Mall S, Ramamurthy G, Rezaizdeh MA. Stress ratio effect on cyclic debonding in adhesively bonded composite joints. *Compos Struct*. 1987;8(1):31-45.
58. Rans CD, Alderliesten RC. Formulating an effective strain energy release rate for a linear elastic fracture mechanics description of delamination growth. *17th International Conferences on Composite Materials* (ICCM17), Edinberg, UK; 2009.
59. Cano AJ, Salazar A, Rodríguez J. Evaluation of different crack driving forces for describing the fatigue crack growth behaviour of PET-G. *Int J Fatigue*. 2018;107:27-32.
60. Pascoe JA, Alderliesten RC, Benedictus R. Towards understanding fatigue disbond growth via cyclic strain energy. *Procedia Mater Sci*. 2014;3:610-615.
61. Pascoe JA, Alderliesten RC, Benedictus R. On the relationship between disbond growth and the release of strain energy. *Eng Fract Mech*. 2015;133:1-13.
62. Pascoe JA, Alderliesten RC, Benedictus R. Characterising resistance to fatigue crack growth in adhesive bonds by measuring release of strain energy. *Proc Struct Integrity*. 2016;2:80-87.
63. Alderliesten RC. How proper similitude can improve our understanding of crack closure and plasticity in fatigue. *Int J Fatigue*. 2016;82:263-273.
64. ASTM E647-15E01. Standard test method for measurement of fatigue crack growth rates. American Society for Testing Materials; 2016.
65. Marinho NR, Arbelo MA, Candido GM, Sales RDCM, Donadon MV. Effects of mean load on interlaminar fracture behavior of carbon-epoxy prepreg fabric laminates under mode I fatigue loading. *Compos Struct*. 2021;276:114451.
66. Kanchanomai C, Thammaruechuc A. Effects of stress ratio on fatigue crack growth of thermoset epoxy resin. *Polym Degrad Stab*. 2009;94(10):1772-1778.
67. Arad S, Radon JC, Culver LE. Fatigue crack propagation in polymethylmethacrylate; the effect of the mean value of stress intensity factor. *J Mech Eng Sci*. 1971;13(2):75-81.
68. Radon JC. Fatigue crack growth in polymers. *Int J Fract*. 1980; 16(6):533-552.

How to cite this article: Sekiguchi Y, Houjou K, Shimamoto K, Sato C. Two-parameter analysis of fatigue crack growth behavior in structural acrylic adhesive joints. *Fatigue Fract Eng Mater Struct*. 2023;46(3):909-923. doi:10.1111/ffe.13908